Determination of mean cluster sizes by fluorescence detection upon site-specific photoexcitation

X. Holzapfel,[1] A. Schrodt,[1] G. Hartmann,[1] L. Marder,[1] P. Schmidt,[1] P. Reiß,[1] A. Ehresmann,[1] A. Hans,[1] and A. Knie[1]

Institute of Physics and Center for Interdisciplinary Nanostructure Science and Technology (CINSaT), University of Kassel, Heinrich-Plett-Strasse 40, 34132 Kassel, Germany

(Dated: 29 January 2020)

Electronic excitations in the valence shell of Ne clusters were studied by fluorescence spectroscopy. The measured fluorescence excitation functions contain information about the nature and number of excitonic states and the mean cluster size of the produced size distribution. Mean cluster sizes were determined by comparing surface and bulk contributions using a multidimensional fitting algorithm, with good agreement to commonly used scaling laws. The influence of different size distributions, which were not considered in previous investigations on homogenous noble gas cluster jets, are implemented into the proposed model. The present work is the first approach using fluorescence spectroscopy for the determination of the mean size of Ne cluster jets created by supersonic expansion.

I. INTRODUCTION

Clusters cover the range between molecular and condensed matter physics. For that reason, cluster size-dependent studies are an excellent way to investigate the evolution of physical properties[1]. An established method for the creation of weakly bound clusters, such as van der Waals clusters, is the supersonic expansion of a gas through a nozzle into vacuum[2]. Many parameters, such as the nozzle temperature and the stagnation pressure in the gas reservoir, influence the mean cluster size $\langle N \rangle$ and the distribution of different cluster sizes in the resulting cluster jet[1]. Knowledge of the mean size of the created size distribution is highly desirable, as different observable characteristics of clusters are highly size dependent[1,3]. A common method to estimate the mean size of cluster jets is the usage of scaling laws. A by now established formalism was introduced by Hagena et al.[4–6]. In this formalism the condensation parameter Γ^*, that includes the conditions of thermal expansion as well as an individual gas constant, the molar enthalpy at 0 K, is introduced[4,7,8]. It is connected to the mean cluster size via an empirical formalism deduced from different experiments[7–9].

In many experiments, the connection between the expansion parameters and the condensation of clusters have been investigated with mass spectrometry being one of the first methods used for the detection of clusters[10]. Electron impact ionization, which is used in many mass spectrometers, typically triggers the fragmentation of clusters, which is a major disadvantage for the determination of the initial mean cluster size[8,11]. Another method to determine the mean cluster size and examine their structure is high energy electron diffraction[12,13]. Being first applied to Ar and later on extended to other noble gases, the experiments already described many different characteristics of cluster beams[2]. However, to understand these characteristics sophisticated simulations are necessary, including the cluster structure and temperature as variables[7]. Other methods for cluster jet characterizations are scattering experiments with atoms which were used to determine the size distribution of large clusters and are well suited for non-destructive characterizations[7,14]. Further investigations were done using x-ray photoelectron spectroscopy[15]. Comparing emission intensities from bulk and surface sites, the mean sizes of homogeneous Ar, Kr, and Xe cluster jets were determined. Although correction models can be used, these experiments suffer from the different attenuation of electrons emitted from different sites in the cluster. Some of the mentioned techniques for characterizing cluster beams require considerable experimental effort, additionally to the purpose of the main experiment[11]. More detailed overviews on available characterization

methods are given in Ref.[7,16].

Since some experiments disclosed significant deviations from the scaling laws, further investigations are desired[9]. Especially for Ne clusters, which are vastly used as prototype systems in cluster experiments, experimental studies on the mean cluster size are scarce[4,5].

Here, we present a complementary method for the experimental determination of the mean size of a Ne cluster jet using the fluorescence intensity ratio from surface and bulk sites and compare the results with the commonly used scaling procedure of Hagena et al.[5]. The proposed method images the created mean cluster size, which is advantageous compared to commonly used mass spectrometers detecting fragmented clusters. The fluorescence yield of Ne cluster jets produced for different expansion conditions is measured as a function of the exciting photon energy in the range of the lowermost excitonic excitations of the Ne valence electrons. These excitations correspond to the atomic $2p^6 \rightarrow 2p^5 3s$ transitions with total angular momenta $j = 3/2$ and $j = 1/2$ labelled without and with prime, respectively. The transitions split into surface and bulk excitons, labelled S and B, and are separated in excitation energy[17]. Furthermore, bulk excitons split into transversal and longitudinal branches, labelled with T and L. A hydrogenic Wannier-Mott model can be used to describe the excitation energies of exciton bands in rare-gas solids and the investigated excitons are typically referred to as $n = 1$ excitons in this model, with the principal quantum number n[18].

Experiments in solid Ne reported one broad surface state at 17.15 eV ($j = 1/2$)[18] with a width of $80 - 300$ meV, which is predicted by theory to consist of three or more different states between $17.21 - 17.43$ eV[19], each with a full width at half maximum (FWHM) of approximately 80 meV[18]. One state has a total angular momentum of $j = 1/2$ and two have an angular momentum of $j = 3/2$ each. We point out that for all predicted Ne surface excitons the transition energies and energetic widths are not spectrally resolved yet due to their overlap in excitation[18,20]. Bulk states at 17.36 eV ($j = 3/2$), 17.50 eV ($j = 1/2$) and 17.75 eV ($j = 1/2$)[18] have been reported, the first two being transversal bulk excitons and the third one a longitudinal bulk exciton. The FWHM of the bulk states is approximately 200 meV[20]. Theory also predicts a longitudinal bulk state for $j = 3/2$[19,21], which has not yet been observed experimentally.

The ratio between the $j = 3/2$ and $j = 1/2$ states for the $n = 1$ excitons is changing when going from atomic to solid states[20,22]. Starting from an atomic oscillator strength ratio of approximately $1 : 10$[23], the experimentally reported solid state ratio of $1 : 1$[22,24] and $1 : 5 - 1 : 10$[18,20] deviates from theory $(1 : 52)$[21]. The reported ratios between the oscillator strengths in solids are varying by one order of magnitude.

Fluorescence spectroscopy is able to directly probe the interior of clusters, whereas for experiments using photoelectron spectrometers the mean free path of bulk electrons has to be considered. Numerous investigations have been performed on the scaling laws for homogeneous Ar and Kr cluster jets, but studies on Ne clusters are still rare. The present work evaluates the validity of the scaling laws for Ne clusters and is organized in the following way: The experimental method will be described in section II followed by the introduction to the proposed model in section III. In section IV we discuss the executed analysis procedures and the obtained results with regard to the number of distinguishable excitonic states and the determined mean cluster size. Section IV summarizes the main results of the study.

II. EXPERIMENT

The experiment was performed at the synchrotron radiation facility SOLEIL (Paris) in multi-bunch operation mode at the PLEIADES beamline[25]. The exciting photon energy was changed stepwise from 16.6 eV to 18.1 eV in $10-50$ meV steps with an exciting photon bandwidth of about 5 meV. In this energy range, the lowest Ne outer valence excitations in clusters are expected[26]. The main set-up consists of three chambers. Ne clusters were formed by supersonic expansion of Ne gas through a pinhole-nozzle of 32 µm diameter into the vacuum. The jet was transferred through a skimmer of 1.5 mm diameter into the interaction chamber, where it was crossed with linearly polarized monochromatic synchrotron radiation. An open-face stack of three micro-channel plates (MCP) similar to the one described in Ref.[27] was used to detect fluorescence photons (VUV) with wavelengths below 120 nm. The detector was placed in the detector chamber, separated from the interaction chamber by an aperture for differential pumping. A series of measurements was carried out with different expansion conditions. The nozzle temperature was varied between 34 K and 100 K and the absolute stagnation pressure between 1 bar and 11 bar.

The scaling parameter Γ^*, as introduced in Ref.[7], was used to predict the mean size of the produced jet:

$$\Gamma^* = \frac{p_0^* d_{eq}^{0.85}}{T_0^{2.2875}} \cdot K_{\mathrm{ch}}, \tag{1}$$

with the expansion pressure p_0^* given in mbar, the equivalent nozzle diameter d_{eq} in µm, and the expansion temperature T_0 in K. K_{ch} is a gas specific constant with the value 185 for Ne[28]. Depending on the value of the scaling parameter, three different empiric formulas are used to

calculate the mean cluster size[7]:

$$\langle N \rangle = \begin{cases} a_0 + a_1\Gamma^* + a_2\Gamma^{*2} + a_3\Gamma^{*3} & ; \quad \Gamma^* \leq 350 \\ 33(\frac{\Gamma^*}{1000})^{2.35} & ; \; 350 \leq \Gamma^* \leq 1800 \\ \exp[c_0 + c_1 \ln(\Gamma^*)^{0.8}] & ; \quad \Gamma^* \geq 1800 \end{cases}, \tag{2}$$

with $a_0 = 2.23$, $a_1 = 7.00 \cdot 10^{-3}$, $a_2 = 8.30 \cdot 10^{-5}$, $a_3 = 2.55 \cdot 10^{-7}$, $c_0 = -12.83$ and $c_1 = 3.51$.

III. MODEL

To determine the mean size of a jet of Ne clusters produced by supersonic expansion, the signal intensity ratio from surface to bulk sites is used. This is achieved by measuring the fluorescence intensity from different sites after resonant photoexcitation directly followed by photon emission as a function of the exciting photon energy. Two assumptions were made: 1) As the Ne atoms are weakly bound by van der Waals forces, we assume that the oscillator strength of surface and bulk atoms is equal[29]. 2) Furthermore, we assume that the surface particles contribute only to the surface and the volume atoms only to excitations of the bulk.

To correlate the surface to bulk signal ratio with the mean cluster size, the geometric structure of the clusters needs to be modeled. Photoelectron spectra of Ne in the mean cluster size range from 40 to 550 atoms revealed the co-existence of icosahedron-based and face-centered cubic (fcc) structures[30]. The contribution from fcc structures to the whole measured signal increases with increasing mean cluster size. According to theoretical studies of the total binding energy the icosahedral structure is favored for small clusters until a certain cluster size is reached[31]. For larger clusters the fcc structure is energetically favored. Furthermore, small $XeNe_N$ clusters are reported to be liquid-like up to a mean cluster size of 200[32,33] and between 200 and 300 atoms the transition from the liquid-like to the solid structure takes place. However, another structural model found no evidence for a structural transition from icosahedral to fcc[34]. Overall, different structures are reported for Ne clusters of different sizes.

Indeed other investigations for other homogenous noble gas clusters, like Ar, exist and report similar structures[2,12,13,35,36].

To set up a model an icosahedral structure with an fcc structure is used as these two structures cover the majority of the investigated mean cluster sizes. Two prominent suggested fcc structures are octahedrons[31] and cuboctahedrons[37]. In the following model, the second structure together

with icosahedron-based structure will be used to determine the mean cluster size[38,39]. The usage of these two structures covers the range of experimentally investigated cluster sizes in the present work.

The total number of particles $N(k)$ of a single icosahedral or cuboctahedral cluster is given by the number of shells $k \geq 1$ the icosahedron/cuboctahedron is built of[40]:

$$N := N(k) = \frac{10k^3 - 15k^2 + 11k - 3}{3} = N_S(k) + N_B(k). \tag{3}$$

The cluster can be divided into a surface with $N_S(k)$ and a bulk with $N_B(k)$ particles, the number of particles being proportional to the intensity of the signals from surface I_S and bulk I_B. The surface portion $S(N)$ of the measured intensity can then be described by

$$S(N) := \frac{I_S}{I_S + I_B} = \frac{N(k) - N(k-1)}{N(k)}. \tag{4}$$

For our analysis, the continuous inverse function of $N(S)$ is needed. Since the analytical invers expression of Eq. 4 is non-trivial, it is numerically approximated by

$$N(S) = q_1 S^{-1} + q_2 S^{-2} + q_3 S^{-3}, \tag{5}$$

with $q_1 = 6.46$, $q_2 = -90.00$, $q_3 = 90.00$.

The supersonic expansion intrinsically creates a distribution of different cluster sizes, which can be described by a log-normal or Gaussian distribution $f_{w,E}(N)$. w is the width of the distribution, in the following represented as full width at half maximum (FWHM), and E the expectation value, which is indeed the mean cluster size $\langle N \rangle$[41–43]. Typically, the FWHM of the size distribution varies between $\langle N \rangle / 2$[9,13] and $\langle N \rangle$[3,29,33,44]. The measured surface ratio $S_m(\langle N \rangle)$ is the integrated signal from all $S(N)$ weighted by the amount of clusters with specific sizes N, given by the distribution $f_{w,\langle N \rangle}(N)$:

$$S_m(\langle N \rangle) = \sum_N f_{w,\langle N \rangle}(N) \cdot S(N). \tag{6}$$

For a monodisperse jet, $N(= \langle N \rangle_{mono})$ can be calculated using Eq. 5.

The experiment does not provide any information about w. However, the influence of different size distributions and their widths on the measured $\langle N \rangle$ can be estimated. Towards this end, we solve Eq. 6 numerically for $\langle N \rangle$ for values of $S_m \in [0.1, 1]$ and by expressing w in terms of $\langle N \rangle$. The resulting $\langle N \rangle (S_m)$ is shown in Fig. 1 for a monodisperse jet and for jets with log-normal and

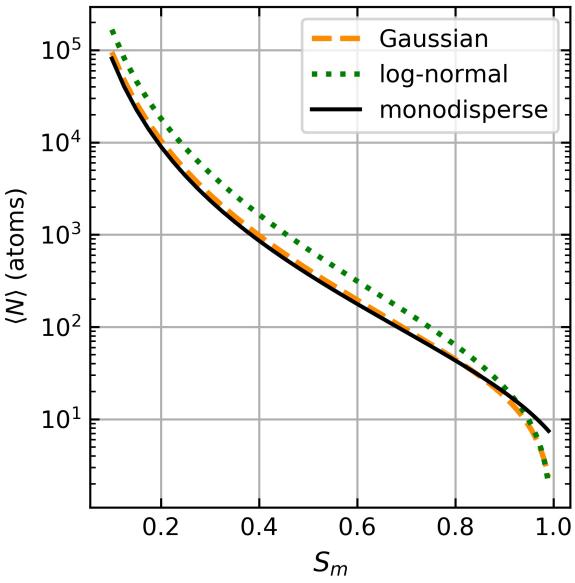

FIG. 1. Calculated cluster size $\langle N \rangle$ as function of the surface portion S_m according to (6) assuming three different size distributions: monodisperse (black, solid line), log-normal with FWHM $=\langle N \rangle$ (green, dotted line), Gaussian with FWHM $=\langle N \rangle$ (orange, dashed line).

Gaussian size distributions of FWHM $=\langle N \rangle$. The method itself shows a high sensitivity for cluster sizes between 10 and 10^4 atoms. Beyond 10^4 atoms, the slope of the surface-to-bulk ratio curve is to steep to yield a sufficient accuracy.

The relative deviations of the expected $\langle N \rangle$ for Gaussian and log-normal distributions of FWHM $=\langle N \rangle$ and $\langle N \rangle/2$ from $N(S)$ of a monodisperse jet are shown in Fig. 2.

In the experiment the measured surface portions S_m are ranging from 0.2 to 0.9. Throughout the following analysis we calculate $N(S_m)$ and subsequently use the correction for a Gaussian distribution with a FWHM of $\langle N \rangle$, as this distribution results in the best agreement between calculated and measured mean cluster sizes, see section IV B.

IV. RESULTS AND DISCUSSION

Within this section all mean cluster sizes are calculated by the procedure described above. Fig. 3 shows an exemplary fluorescence yield as a function of the exciting photon energy for a mean cluster size of 1052 atoms. An optimized fit of the four distinct features with four Gaussian functions is depicted. An iterative global fitting procedure (as described in the appendix) is applied

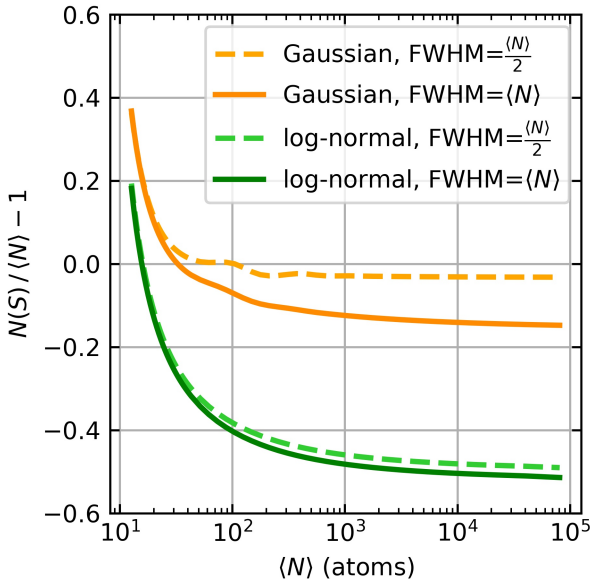

FIG. 2. Relative deviation of the simulated mean cluster sizes from a monodisperse cluster jet for a Gaussian (orange) and log-normal distribution (green) with widths of FWHM $= \langle N \rangle$ (solid) and FWHM $= \langle N \rangle / 2$ (dashed).

on the full set of measurements for different cluster sizes. In Fig. 4 a) the measured fluorescence yield is shown for the produced mean cluster sizes, the positions of surface and bulk states are indicated according to Ref.[18,19,22]. Exemplary fitting results are shown in Fig. 4 b) for a fitting procedure using four different Gaussian functions, one for each state. The fitting results agree very well with the experimental data as can be seen in Figs. 3 and 4.

A. Cluster size dependent trends

As described in the introduction, four different excitonic states have been reported experimentally (three bulk and one surface states) and the spectral positions of two additional surface and one bulk states have been predicted by theory.

The results of the global fit are shown in Fig. 5. Panel a) depicts the evolution of the transition energies with growing cluster size for the four Gaussian functions. Dashed lines indicate the solid state literature values for the literature assigned states: one surface state with (S') and three bulk states (B), two transversal (denoted with a subletter T) and one longitudinal (denoted with a subletter L). Panel b) shows the relative contribution of each Gaussian (G_1 to G_4) to the total

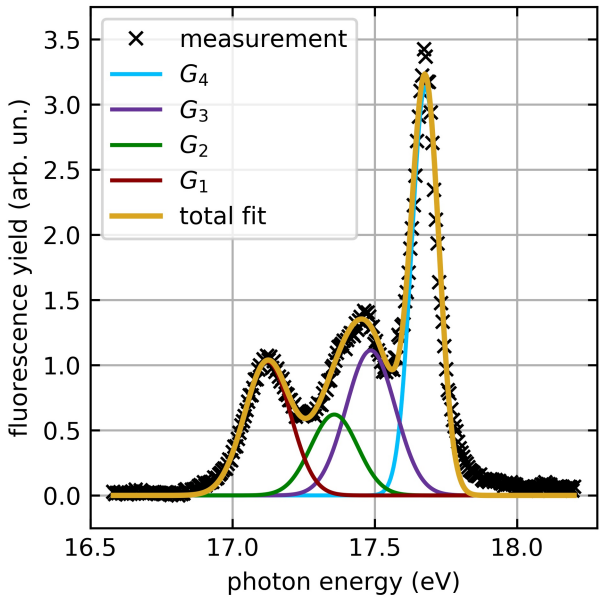

FIG. 3. Examplary fluorescence yield as a function of the exciting photon energy for a mean cluster size of 1052 atoms. The solid yellow line depicts the total fit of the experimental results by the sum of four Gaussian functions, representing four excitonic states.

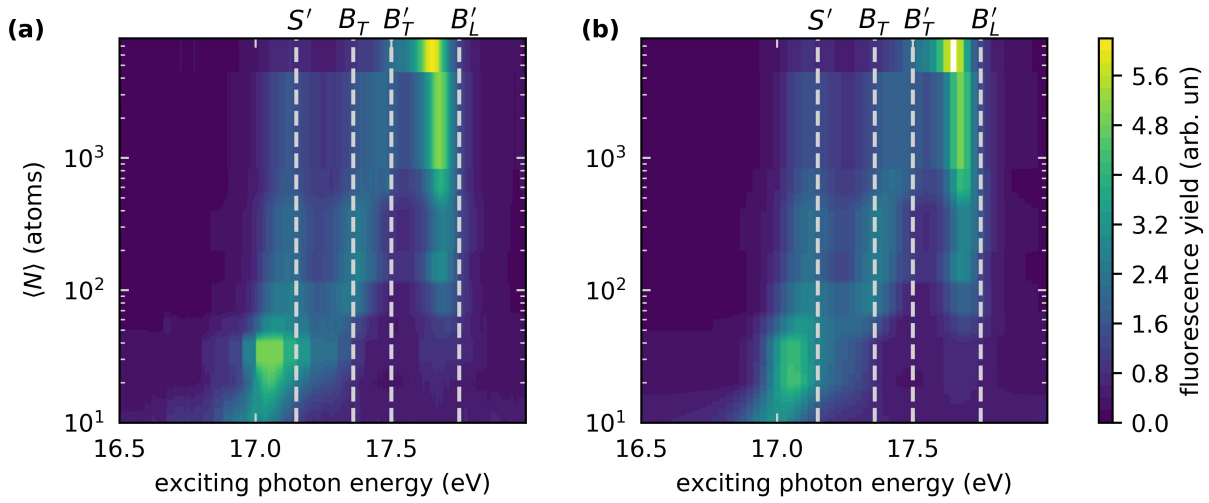

FIG. 4. a) Measured fluorescence yield as function of the exciting photon energy for the complete set of investigated mean cluster sizes, b) corresponding global fitting results (see appendix). Dashed lines indicate the values of experimentally observed states as reported in the literature (see text for details).

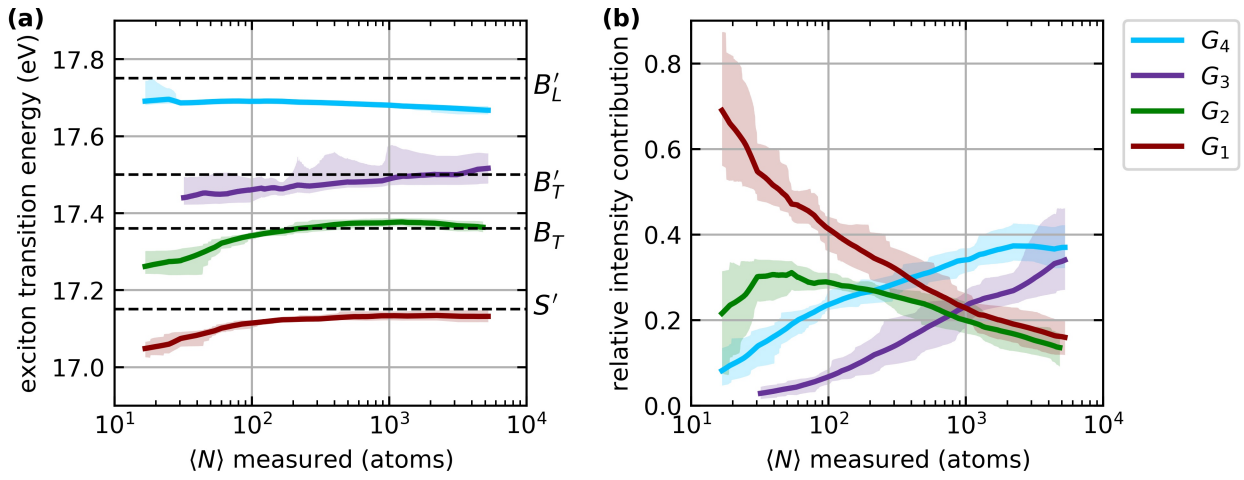

FIG. 5. Global fit results of the fluorescence yields for the investigated cluster sizes. a) Transition energies of the four Gaussians G_1 to G_4 are depicted with their respective colors. Dashed lines indicate the solid state literature values for the literature assigned states. b) Relative intensity contributions. For intensity contribution below 0.03 the results are not displayed. The uncertainties of the fit procedure are given by the shaded areas (see appendix for details).

fluorescence yield.

The transition energy of G_1 converges to the solid state literature value of the surface exciton S'[18] and its relative intensity contribution decreases with increasing cluster size, as expected for a surface state. Analogously, the transition energy of G_3 converges to the solid state literature value of the bulk exciton B'_T[18] and its relative intensity contribution increases with increasing cluster size, as expected for a bulk state. Except for a slight deviation from the solid state transition energy, G_4 can be interpreted as B'_L. In contrast, G_2 behaves ambigously. While its transition energy converges to that of the reported value for B_T, its relative intensity contribution corresponds to a surface state. Due to the uncertainty of G_2 for very small clusters a reliable interpretation in this size range is not reasonable. Our interpretation of G_2 beeing a surface state is in agreement with investigations on heterogeneous clusters by Kanaev et al.[45]. They report only two observable bulk states.

The size dependent transition energy shift of G_1-G_3 is in accordance to existing models[43,46] and the opposite trend of G_4 is known in literature[3,47].

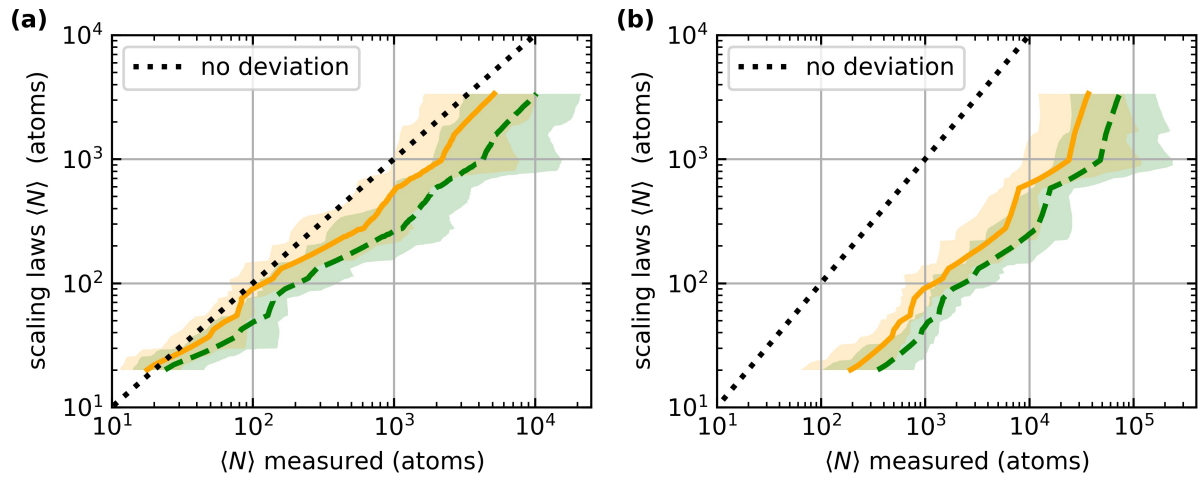

FIG. 6. Comparison of mean cluster sizes determined by the scaling laws and the procedure described above. Mean cluster size for a Gaussian (orange, solid) and a log-normal (green, dashed) cluster size distribution. The uncertainty region of the fit procedure is given by the shaded area.

B. Measured mean cluster sizes

For each set of experimental conditions we calculated the mean cluster size $\langle N \rangle$ from the fluorescence yield results according to the procedure described above. In Fig. 6 these cluster sizes are compared to the cluster sizes determined by the scaling laws[7]. Due to the ambiguous assignment of G_2 two variants of the mean cluster size determinations were performed. Panel a) shows the comparison taking into account our new assignment of G_2 as a surface state. In panel b) the literature assignment is used. For both versions log-normal (green) and Gaussian (orange) cluster size distributions are displayed. As the agreement within the uncertainty is undoubtly much better for our new assignment, we propose to reassign the state accordingly.

V. CONCLUSION

We used polyicosahedral and cuboctahedral structural models to determine the mean cluster size within a jet of condensed Ne atoms. The ratio of surface to bulk atoms was obtained from fluorescence excitation spectra in the range of the Ne valence excitonic states and converted to mean cluster sizes. The significant influence of different size distributions was quantified and included into the model. Our analysis of the excitation spectra revealed characteristic behavior

of surface and bulk excitonic states. We propose the reasignment of one bulk state into a surface state. Only including this reassignment, the final results show a remarkably good agreement with semi empirical scaling laws.

VI. ACKNOWLEDGMENTS

The work was partially supported by a grant from the Otto-Braun-Fonds (Melsungen) and the GSI Helmholtzzentrum für Schwerionenforschung (Darmstadt). We acknowledge the PLEIADES beamline team and the SOLEIL staff for excellent support during the experiments.

REFERENCES

[1] J. Jortner, Zeitschrift für Physik D Atoms, Molecules and Clusters **24**, 247 (1992).

[2] J. Farges, M. F. de Feraudy, B. Raoult, and G. Torchet, Surface Science **106**, 95 (1981).

[3] J. Wörmer, R. Karnbach, M. Joppien, and T. Möller, Journal of Chemical Physics **104**, 8269 (1996).

[4] O. F. Hagena and W. Obert, Journal of Chemical Physics **56**, 1793 (1972).

[5] O. F. Hagena, Surface Science **106**, 101 (1981).

[6] O. F. Hagena, Zeitschrift für Physik D Atoms, Molecules and Clusters **4**, 291 (1987).

[7] U. Buck and R. Krohne, Journal of Chemical Physics **105**, 5408 (1996).

[8] R. Karnbach, M. Joppien, J. Stapelfeldt, J. Wörmer, and T. Möller, Review of Scientific Instruments **64**, 2838 (1993).

[9] H. Bergersen, M. Abu-Samha, J. Harnes, O. Björneholm, S. Svensson, L. J. Sæthre, K. J. Børve, M. Abu-Samha, and L. J. Saethre, Physical Chemistry Chemical Physics **8**, 1891 (2006).

[10] W. Henkes, Zeitschrift fur Naturforschung - Section A Journal of Physical Sciences **16**, 842 (1961).

[11] A. J. Bell, J. M. Mestdagh, J. Berlande, X. Biquard, J. Cuvellier, A. Lallement, P. Meynadier, O. Sublemontier, and J.-P. Visticot, Journal of Chemical Physics **26**, 994 (1993).

[12] J. Farges, M. F. de Feraudy, B. Raoult, and G. Torchet, Journal of Chemical Physics **78**, 5067 (1983).

[13] J. Farges, M. F. de Feraudy, B. Raoult, and G. Torchet, Journal of Chemical Physics **84**, 3491 (1986).

[14]J. Gspann and H. Vollmar, pp. 261–267.

[15]M. Tchaplyguine, R. R. Marinho, M. Gisselbrecht, J. Schulz, N. Mårtensson, S. L. Sorensen, A. N. de Brito, R. Feifel, G. Ohrwall, M. Lundwall, S. Svensson, and O. Björneholm, The Journal of Chemical Physics **120**, 345 (2004).

[16]E. L. Knuth, Journal of Chemical Physics **107**, 9125 (1997).

[17]N. Schwentner, E. E. Koch, and J. Jortner, 1st ed., Vol. 107 (Springer Berlin Heidelberg, 1985).

[18]V. Saile and E. E. Koch, Physical Review B **20**, 784 (1979).

[19]V. Chandrasekharan and E. Boursey, Physical Review B **19**, 3299 (1979).

[20]V. Saile and E. E. Koch, Physical Review B **21**, 4892 (1980).

[21]W. Andreoni, F. Perrot, and F. Bassani, Physical Review B **14**, 3589 (1976).

[22]E. Boursey, M. C. Castex, V. Chandrasekharan, and M.-C. Castex, Physical Review B **16**, 2858 (1977).

[23]W. F. Chan, G. Cooper, X. Guo, and C. E. Brion, Physical Review A **45**, 1420 (1992).

[24]D. Pudewill, F. J. Himpsel, V. Saile, N. Schwentner, M. Skibowski, E. E. Koch, and F.-J. Himpsel, Physica Status Solidi (B) **74**, 485 (1976).

[25]A. Hans, L. Ben Ltaief, M. Förstel, P. Schmidt, C. Ozga, P. Reiß, X. Holzapfel, C. Küstner-Wetekam, F. Wiegandt, F. Trinter, U. Hergenhahn, T. Jahnke, R. Dörner, A. Ehresmann, P. V. Demekhin, and A. Knie, Chemical Physics **482**, 165 (2017).

[26]O. Björneholm, F. Federmann, M. Joppien, F. Fössing, S. Kakar, R. von Pietrowski, and T. Möller, Surface Review and Letters **03**, 299 (1996).

[27]A. Hans, P. Schmidt, C. Ozga, G. Hartmann, X. Holzapfel, A. Ehresmann, and A. Knie, Materials **11**, 1 (2018).

[28]J. Wörmer, V. Guzielski, J. Stapelfeldt, and T. Möller, Chemical Physics Letters **159**, 321 (1989).

[29]J. Stapelfeldt, J. Wörmer, and T. Möller, Physical Review Letters **62**, 98 (1989).

[30]S. Joshi, S. Barth, S. Marburger, V. Ulrich, and U. Hergenhahn, European Physical Journal D **73**, 343 (2006).

[31]B. W. van de Waal, Journal of Chemical Physics **98**, 4909 (1993).

[32]R. von Pietrowski, M. Rutzen, K. von Haeften, S. Kakar, and T. Möller, Zeitschrift für Physik D Atoms, Molecules and Clusters **40**, 22 (1997).

[33]R. von Pietrowski, K. von Haeften, T. Laarmann, T. Möller, L. Museur, and A. V. Kanaev, European Physical Journal D **38**, 323 (2006).

[34]B. W. van de Waal, Physical Review Letters **76**, 1083 (1996).

[35]O. Echt, K. Sattler, and E. Recknagel, Physical Review Letters **47**, 1121 (1981).

[36]S. Kakar, O. Björneholm, J. Weigelt, A. R. B. de Castro, L. Tröger, R. Frahm, T. Möller, A. Knop, and E. Rühl, Physical Review Letters **78**, 1675 (1997).

[37]B. Raoult, J. Farges, M. F. de Feraudy, and G. Torchet, Philosophical Magazine B: Physics of Condensed Matter; Statistical Mechanics, Electronic, Optical and Magnetic Properties **60**, 881 (1989).

[38]A. L. Mackay, Acta Crystallographica **15**, 916 (1962).

[39]B. K. Teo and N. J. A. Sloane, Inorganic Chemistry **24**, 4545 (1985).

[40]R. L. Johnston, Masters series in physics and astronomy (Taylor & Francis, 2002).

[41]M. Lewerenz, B. Schilling, and J. P. Toennies, Chemical Physics Letters **206**, 381 (1993).

[42]K. Y. Kim, V. Kumarappan, and H. M. Milchberg, Applied Physics Letters **83**, 3210 (2003).

[43]C.-R. Wang, R.-B. Huang, Z.-Y. Liu, and L.-S. Zheng, Chemical Physics Letters **227**, 103 (1994).

[44]J. Wörmer, M. Joppien, and T. Möller, Chemical Physics Letters **182**, 632 (1991).

[45]A. Kanaev, L. Museur, F. Edery, T. Laarmann, and T. Möller, Physical Review B - Condensed Matter and Materials Physics **69**, 2654 (2004).

[46]L. E. Brus, Journal of Chemical Physics **80**, 4403 (1984).

[47]T. Laarmann, K. von Haeften, A. Kanaev, H. Wabnitz, and T. Möller, Physical Review B - Condensed Matter and Materials Physics **66**, 1 (2002).

Appendix A: Fitting Algorithm

The fitting algorithm uses the Python environment and is an iterative fit of multiple Gaussian functions to the measured excitation spectra. The number of Gaussians is defined by the number of assumed excitonic states.

A single run of the iterative fit consists of the three following steps:

1) As initialization step from the measured spectra a subset is chosen randomly and sorted in the order of mean cluster sizes calculated by the scaling laws (2).

2) On the spectra subset four different optimizations are performed.

Each of the four optimizations starts with the fitting of a spectrum with a given mean cluster size. After the fitting of the spectrum is finalized, the next spectrum with either higher or lower mean cluster size will be analyzed. The previously obtained fitting parameters are used as initial

parameters for the fitting of the next spectrum. This process is performed iteratively until the analysis of the last spectrum is finished. The four optimizations differ in the starting spectrum's mean cluster size and the optimization direction of the algorithm:

a) starting from the smallest to the highest mean cluster size,

b) starting from the highest to the smallest mean cluster size,

c) starting from the average to the highest mean cluster size,

d) starting from the average to the lowest mean cluster size.

3) The mean cluster sizes are calculated using the fitting results from the second step and the spectra are reordered according to these newly obtained sizes. Now the algorithm starts at 1) for a second iteration using the reordered spectra. After the second iteration is finished the resulting parameters are used for the presented analysis.

A subset of the measured spectra is used to obtain a variation of the fitting algorithm and the results. The iterative fit 1) to 3) is therefore used multiple times with different randomly chosen samples. As the algorithm performs several slightly different optimizations of one spectrum, it results in multiple parameters for each spectrum.

To get the major trend of these parameters, the moving average is calculated over all results. For all parameters below the moving average of all results a separate moving average is calculated in the same predefined range. This separate moving average is used as lower uncertainty limit. The upper uncertainty limit is also analogously calculated, for all parameters above the moving average of all results. The upper and lower uncertainty limits are illustrated as uncertainty region by shaded areas.